Int. J. Therm. Sci. (2000) 39, 39–52

S1290-0729(00)00190-2/FLA

Study of the behaviour of a bubble in an electric field: steady shape and local fluid motion

Mohamed Chaker Zaghdoudi [a], Monique Lallemand [b]*

[a] *Centre de Thermique, UPRESA CNRS 5008, INSA, 20 Av. Albert Einstein, 69621 Villeurbanne, France*

[b] *Centre de Thermique, UPRESA CNRS 5008, Institut National des Sciences Appliquées, INSA, 20 Av. Albert Einstein, 69621 Villeurbanne, France*

(Received 4 January 1999, accepted 30 July 1999)

Abstract — The aim of this study is to investigate the effects of a uniform electric field on bubbles. Numerical analyses have been carried out in order to determine the shape of an axisymmetric conducting bubble immersed in an isothermal dielectric fluid. A detailed analysis of the interfacial electric stresses acting on the liquid–vapour conducting interface is discussed. This study shows a deformation of the bubble in the electric field direction and also electroconvective movements within and around the conducting bubble. The electroconvective movements are analysed on the basis of the creeping flow approximation. A comparison between the conducting bubble shape and the dielectric bubble one is also presented. © 2000 Éditions scientifiques et médicales Elsevier SAS

bubble / heat transfer enhancement / electrohydrodynamic effect / electric field

Résumé — **Etude du comportement d'une bulle dans un champ électrique : forme de la bulle et mouvement local du fluide.** Cet article concerne l'étude des effets d'un champ électrique uniforme sur une bulle. La forme d'une bulle conductrice axisymétrique, au sein d'un fluide diélectrique uniforme, a été calculée numériquement. Une analyse détaillée des contraintes interfaciales agissant sur l'interface conductrice liquide–vapeur est présentée. Cette étude montre une déformation de la bulle dans la direction du champ électrique et met en évidence le rôle des mouvements électroconvectifs à l'intérieur et autour de la bulle. Ces mouvements électroconvectifs ont été déterminés en supposant un écoulement rampant. Une comparaison entre les formes des bulles conductrices et diélectriques est aussi présentée. © 2000 Éditions scientifiques et médicales Elsevier SAS

bulle / augmentation des échanges thermiques / effet électrohydrodynamique / champ électrique

Nomenclature

a	thermal diffusivity	$m^2 \cdot s^{-1}$
$\boldsymbol{D}$	electric displacement vector	$F \cdot V \cdot m^{-2}$
$\boldsymbol{e}_r, \boldsymbol{e}_\theta$	unit radial and orthoradial vectors	
E	electric field strength	$V \cdot m^{-1}$
f_s	electric stress	$N \cdot m^{-2}$
f_v	volume force	$N \cdot m^{-3}$
f_{vis}	viscous stress	$N \cdot m^{-2}$
g	gravitational acceleration	$m \cdot s^{-2}$
$\boldsymbol{j}$	current density	$A \cdot m^{-2}$
$\boldsymbol{n}$	unit normal vector	
P	pressure	Pa
P_n	Legendre polynomial	
q_s	electrical surface charge density	$C \cdot m^{-2}$
q_v	electrical volume charge density	$C \cdot m^{-3}$
r	radial coordinate	m
r^*	dimensionless radius	
R	bubble radius	m
Re	Reynolds number	
$\boldsymbol{t}$	unit tangential vector	
t_c	characteristic time	s
u	radial velocity	$m \cdot s^{-1}$
u^*	dimensionless radial velocity $= u/U^*$	
U^*	maximum liquid velocity	$m \cdot s^{-1}$
v	orthoradial velocity	$m \cdot s^{-1}$
v^*	dimensionless orthoradial velocity $= v/U^*$	
V	electrical potential	V
X	$= \rho_{el}/\rho_{ev}$	
Y	$= \varepsilon_{rl}/\varepsilon_{rv}$	

Greek symbols

ε	dielectric permittivity	$F \cdot m^{-1}$
ε_0	vacuum dielectric permittivity	$F \cdot m^{-1}$

* Correspondence and reprints.
m.lal@cethil.insa-lyon.fr

ε_r	relative dielectric permittivity	
μ	dynamic viscosity	Pa·s
μ^*	dimensionless coordinate $= \cos\theta$	
θ	angular coordinate	
ρ_e	electrical resistivity	Ω·m
ρ	density	kg·m^{-3}
σ	surface tension	N·m^{-1}
σ_e	electrical conductivity	Ω^{-1}·m^{-1}
τ	relaxation time	s
ψ	stream function	
$\zeta(\theta)$	bubble deformation	m
ζ^*	dimensionless coordinate $= \zeta / R$	

Subscripts

j	liquid or vapour
l	liquid
n	normal
0	applied electric field
t	tangential
v	vapour
x	horizontal component
z	vertical component

1. INTRODUCTION

An electric field can be an efficient method to enhance nucleate boiling heat transfer [1, 2]. The Electro-HydroDynamical (EHD) boiling process has been used in many industries such as in refrigerating units [3]. Large enhancements have been achieved by Ohadi [4] in a shell-and-tube heat exchanger. The great interest in use of the electric field in conjunction with boiling results from: (i) the nucleate pool boiling heat transfer enhancement [5], (ii) the increase of the Critical Heat Flux (CHF) [6], (iii) the elimination of boiling hysteresis [7], and (iv) film boiling has been found to be deferred to higher values in presence of an electric field [8].

Several fundamental studies have been carried out in order to understand the basic mechanisms. In these studies, the electric field effects on the bubbles have been particularly studied because the change in the bubble behaviour in the presence of an electric field is one of the main reasons for the heat transfer enhancement. The experimental and theoretical researches can be classified into two groups.

The first group deals with the electric field effect on bubbles or drops immersed in an isothermal dielectric medium. Garton and Krasucki [9] have shown that a bubble, subjected to an electric field between two parallel plate electrodes, assumes the shape of a prolate spheroid in the direction of the field. They show that bubbles, for which the dielectric permittivity exceeds twenty times the medium permittivity, elongate until a critical shape is reached, then bubbles become unstable. Bubbles of dielectric permittivity ratio lower than 20 elongate indefinitely when the electric field increases. Miksis [10] shows theoretically that, when the dielectric permittivity of a drop is larger than a critical value, the drop develops two obtuse-angled conical points at its ends for a certain electric field strength. For dielectric permittivities lower than the critical value, the drop elongates and keeps its nearly prolate spherical shape without developing conical points as the field is increased.

The second group deals with the electric field effect on bubbles attached to a wall in isothermal conditions [11–14] or non-isothermal conditions [15, 16]. Cheng and Chaddock [11] extended the Fritz's analysis on maximum bubble volume during boiling under zero-field conditions to the EHD conditions. They found that the bubble departure size decreases as the electric field strength or the dielectric permittivity of the fluid increase. Ogata and Yabe [12] have obtained the following conclusions from experimental results: the bubbles in the electric field are pushed against the grounded wall by the vertical component of the electric stresses and move horizontally due to the horizontal component. They attribute this effect to the fact that the horizontal component of the electric stresses is more than four times larger than the vertical component. More recently, Cho et al. [13] have investigated numerically and experimentally the effects of uniform DC electric fields on a bubble attached to a wall. In their numerical analysis, the bubble is found to be extended in a direction parallel to the applied electric field. The elongation increases as the electric field strength increases. Consequently, the contact angle also increases with an increase of the electric field strength if the contact radius is fixed. If the contact angle is fixed, the contact radius decreases as the electric field strength increases. Moreover, Kweon et al. [14] studied experimentally the effect of the uniformity of the electric field on the deformation and the departure volume of a bubble under DC/AC electric field. For DC electric field, the bubble departure volume in a nonuniform electric field decreases continuously, while in a uniform electric field it remains nearly constant. For AC electric field, the departure process of a bubble is associated with the bubble oscillation and the applied voltage. The bubble departure volume drops suddenly near a critical voltage and the decrease of the bubble departure volume is greater in an AC than in a DC electric field. By considering the presence of the thermal boundary layer, Ogata et al. [15, 16] showed that, for a bubble deformed in an electric field, the area of the thin liquid film

at the bottom of the bubble is enlarged. An analytical simulation indicates that this shape is due to the weaker electric field strength in the thermal boundary layer than in the saturated region, resulting in a weaker electric stress.

In spite of the large number of studies on the bubble behaviour, the bubble elongation under an electric field has often been considered assuming a liquid–vapour interface without electrical free charges. However, although the electrical conductivity of either phase is small, the charge associated with steady currents adds up at the interface till the steady state is achieved. In the present study, the effects of an electric field on the bubble in the presence of electrical free charges at the liquid–vapour interface is considered. For this purpose, the effects of electrical parameters, such as electrical conductivity, dielectric permittivity and the electric field strength on the bubble shape are investigated under isothermal conditions.

2. ELECTROHYDRODYNAMIC EQUATIONS

With EHD phenomena, the basic momentum and energy equations are modified by appropriate terms. They are written with in addition the electrical equations and appropriate boundary conditions for an incompressible fluid with the purpose of outlining the main physical aspects and the importance of the assumptions. We will distinguish equations that are relative to the electrodynamic aspect and those relative to the hydrodynamic one.

2.1. Electrodynamic equations

Let us consider the basic electrical laws defining the problem. A prominent feature of electrohydrodynamic interactions is the fact that the electric field, E, is irrotational. Dynamic currents are so small that the magnetic induction is negligible and the appropriate laws are mainly those of electrostatics, as summarised below:

$$\operatorname{curl} \boldsymbol{E} = 0 \tag{1}$$

$$\boldsymbol{D} = \varepsilon \boldsymbol{E} \tag{2}$$

$$\nabla \cdot \boldsymbol{D} = q_{\mathrm{v}} \tag{3}$$

$$\boldsymbol{j} = \sigma_{\mathrm{e}} \boldsymbol{E} + q_{\mathrm{v}} \boldsymbol{u} + \frac{\partial \boldsymbol{D}}{\partial t} \tag{4}$$

$$\nabla \cdot \boldsymbol{j} = 0 \tag{5}$$

TABLE I
Relaxation time for different dielectric fluids.

Fluid	P (bar)	T_{sat} (°C)	$\varepsilon_{\mathrm{rl}}$	λ_{e} ($\Omega^{-1}\cdot\mathrm{m}^{-1}$)	τ (s)
n-pentane	1	36	1.80	$6.7\cdot10^{-9}$	$2.4\cdot10^{-3}$
R-113	1	47	2.40	$1\cdot10^{-11}$	2.12
R-123	1	28	3.42	$3.4\cdot10^{-8}$	$0.9\cdot10^{-3}$

In equation (3), the electrical free charges density q_{v} are expressed in terms of the electric displacement $\boldsymbol{D}$. The current density is the sum of three terms: the first term, $\sigma_{\mathrm{e}}\boldsymbol{E}$, is the contribution of the electrical conduction in the medium, the second term, $q_{\mathrm{v}}\boldsymbol{u}$, is due to the free charge convection and the third term is due to the electric displacement variations with time. The conservation of free charges is expressed by equation (5).

Even though electrical conduction in fluids is often poorly characterised by the Ohm law ($\boldsymbol{j} = \sigma_{\mathrm{e}}\boldsymbol{E}$), this simple conduction law can be used to make some important conclusions. By considering equations (2)–(5) written for the steady state, an equation for the electrical free charge density is obtained

$$q_{\mathrm{v}} = \frac{1}{\tau}\boldsymbol{D} \cdot \nabla\tau \tag{6}$$

This equation shows that the appearance of the electrical free charges is due to a gradient of the quantity $\tau = \varepsilon/\sigma_{\mathrm{e}}$ which is a characteristic of a fluid. The relaxation time, τ, represents the time needed by a free charge to relax from the fluid to its external boundary (liquid–vapour interface for example). From the relaxation time, we can determine if the liquid behaves like an insulating fluid or not by comparing its value to the dynamically characteristic time t_{c} which can be the period of the imposed electric field [17], the period of the mechanical oscillations of a liquid–vapour interface [18], the detachment period of bubbles [5], etc. Then, if $t_{\mathrm{c}} \ll \tau$, the fluid can be considered as highly insulating and the electric field is distributed within both the liquid and the vapour. In this case, no electrical free charges appear within either the media or the liquid–vapour interface. At the opposite, if $t_{\mathrm{c}} \gg \tau$, the electric field is totally excluded from the liquid, which behaves as a conducting fluid, and the entire voltage drop occurs at the liquid–vapour interface where electrical free charges appear. The values of τ for some dielectric fluids are shown in *table I*.

2.2. Hydrodynamic equations

The set of equations written for an incompressible fluid is as follows:

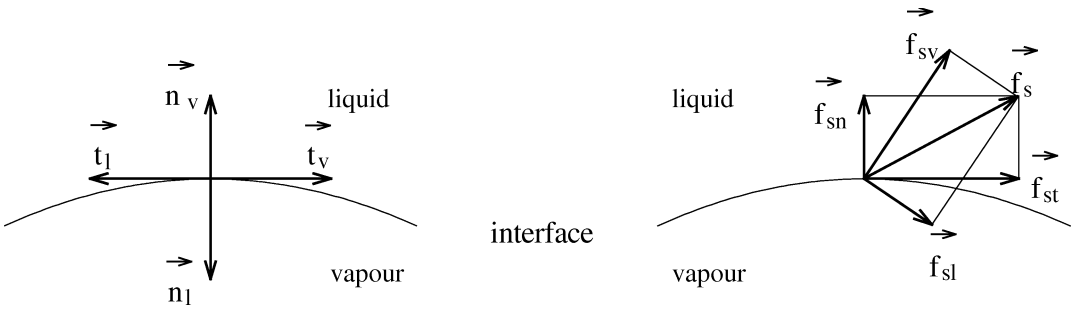

Figure 1. Electric stresses acting on an interface.

$$\nabla \cdot \boldsymbol{u} = 0 \tag{7}$$

$$\rho \frac{\mathrm{D}\boldsymbol{u}}{\mathrm{D}t} = -\nabla P + \boldsymbol{f}_\mathrm{v} + \rho \boldsymbol{g} + \mu \nabla^2 \boldsymbol{u} \tag{8}$$

$$\frac{\mathrm{D}T}{\mathrm{D}t} = a\nabla^2 T + \frac{\sigma_\mathrm{e} E^2}{\rho c_\mathrm{p}} \tag{9}$$

$\mathrm{D}T/\mathrm{D}t$ is termed the material derivative.

The momentum equation (8) involves an additional term, which represents the electric force acting on the fluid. This force is due, on the one hand, to the electrical free charges that contribute to conduction and to convection currents, on the other hand, to the polarisation of the medium. This force is given by [19]

$$\boldsymbol{f}_\mathrm{v} = q_\mathrm{v}\boldsymbol{E} - \frac{1}{2}E^2\nabla\varepsilon + \frac{1}{2}\nabla\left(\rho\frac{\partial\varepsilon}{\partial\rho}E^2\right) \tag{10}$$

The first term is the Coulomb force exerted on the space electric charges within the dielectric fluid. The second term is the dielectrophoretic force due to the spatial gradient of the dielectric permittivity in the fluid. Physically, this force acts on polarisation charges appearing in the dielectric medium under the electric field effect. The third term is the electrostriction force due to the variation of the dielectric permittivity with the density and to the nonuniformity of the electric field in the medium. The expression of the electrostriction force can be simplified in the case of nonpolar fluids by using the Clausius–Mossotti law

$$\rho\frac{\partial\varepsilon}{\partial\rho} = \frac{(\varepsilon-1)(\varepsilon+2)}{3\varepsilon_0} \tag{11}$$

In order to study the electric force effect on an interface between two fluids, the electric force $\boldsymbol{f}_\mathrm{v}$ can be expressed as a stress (Maxwell stress) by using the Gauss' theorem as follows [19]:

$$\boldsymbol{f}_{\mathrm{s}j} = \varepsilon_j(\boldsymbol{n}\cdot\boldsymbol{E})_j\cdot\boldsymbol{E}_j - \frac{\varepsilon_j}{2}E_j^2\left(1-\frac{\rho}{\varepsilon}\frac{\mathrm{d}\varepsilon}{\mathrm{d}\rho}\right)_j\boldsymbol{n}_j \tag{12}$$

where j is the liquid or the vapour subscript and $\boldsymbol{n}_j$ is the unit normal component in each phase.

The liquid–vapour interface is submitted to the resultant of two stresses (*figure 1*), that is

$$\boldsymbol{f}_\mathrm{s} = \boldsymbol{f}_\mathrm{sl} + \boldsymbol{f}_\mathrm{sv} \tag{13}$$

Rearranging this equation yields the following expressions for the normal and tangential components of the electric stress (see Appendix):

$$\boldsymbol{f}_\mathrm{sn} = \frac{1}{2}\Big[\varepsilon_\mathrm{l}\big(E_\mathrm{ln}^2 - E_\mathrm{lt}^2\big) - \varepsilon_\mathrm{v}\big(E_\mathrm{vn}^2 - E_\mathrm{vt}^2\big) + \rho_\mathrm{l}\frac{\mathrm{d}\varepsilon_\mathrm{l}}{\mathrm{d}\rho_\mathrm{l}}E_\mathrm{l}^2 - \rho_\mathrm{v}\frac{\mathrm{d}\varepsilon_\mathrm{v}}{\mathrm{d}\rho_\mathrm{v}}E_\mathrm{v}^2\Big]\boldsymbol{n}_\mathrm{l} \tag{14}$$

$$\boldsymbol{f}_\mathrm{st} = (\varepsilon_\mathrm{l}E_\mathrm{ln}E_\mathrm{lt} - \varepsilon_\mathrm{v}E_\mathrm{vn}E_\mathrm{vt})\boldsymbol{t}_\mathrm{l} = (\varepsilon_\mathrm{l}E_\mathrm{ln} - \varepsilon_\mathrm{v}E_\mathrm{vn})E_\mathrm{vt}\boldsymbol{t}_\mathrm{l} = q_\mathrm{s}E_\mathrm{vt}\boldsymbol{t}_\mathrm{l} \tag{15}$$

where $\boldsymbol{n}_\mathrm{l}$ is the unit normal vector directed towards the liquid phase and $\boldsymbol{t}_\mathrm{l}$ is the tangential vector to the liquid–vapour interface. q_s is the electrical charge density appearing at the liquid–vapour interface due to the electric field strength imbalance along the liquid–vapour interface.

The tangential component (equation (5)) is the Coulomb stress generated on the liquid–vapour interface by the electric field. When a fluid in a two-phase system is considered as perfectly insulating, there is no free charge density acting on the liquid–vapour interface and only the normal component of the electric stress acts on the interface. For a more conducting fluid, the liquid–vapour interface can be regarded as perfectly conducting and the electric field has only a normal component. By contrast with these two limiting cases, tangential electric stresses act on the liquid–vapour interface. This latter case is the subject of this study.

3. ELECTRIC STRESSES ACTING ON A CONDUCTING BUBBLE

The analysis of the effect of the electric stresses on the liquid–vapour interface requires the knowledge of the electric field distribution around and within a conducting bubble.

3.1. Electric field distribution within and around a conducting bubble

The electric potential distribution for a spherical conductor immersed in an other conductor is known [19]. If ρ_{el} and ρ_{ev} are the electrical resistivities of the liquid and the vapour phases, respectively, R the radius of the bubble and E_0 the uniform electric field far from the bubble, the electric potentials V_l and V_v outside and inside the bubble are expressed in spherical coordinates (*figure 2*) as follows:

$$V_l = -E_0 \cos\theta \left[r + \frac{1-X}{2+X} \frac{R^3}{r^2} \right] \tag{16}$$

$$V_v = -\frac{3E_0 r \cos\theta}{2+X} \tag{17}$$

where $X = \rho_{el}/\rho_{ev}$.

From the above equations, the electric field distribution in the liquid and the vapour phases can be obtained.

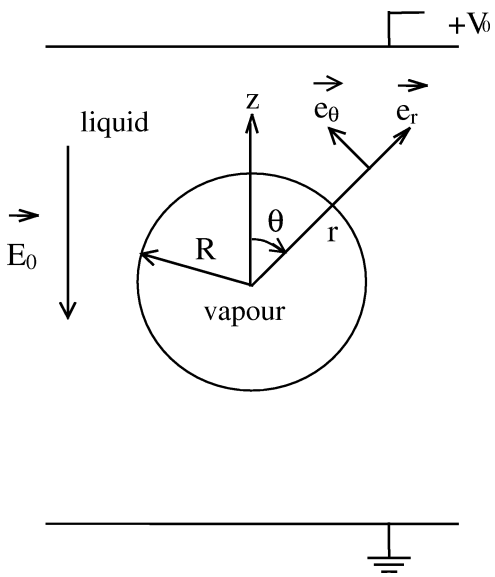

Figure 2. Freely bubble immersed in a dielectric medium in EHD conditions.

In the liquid phase, the normal and the tangential components of the electric field are

$$E_{ln} = E_0 \cos\theta \left[1 - \frac{2(1-X)}{2+X} \frac{R^3}{r^3} \right] \tag{18}$$

$$E_{lt} = -E_0 \sin\theta \left[1 + \frac{1-X}{2+X} \frac{R^3}{r^3} \right] \tag{19}$$

For the vapour side, these components are

$$E_{vn} = -\left(\frac{\partial V_v}{\partial r} \right)_{r=R} = \frac{3E_0 \cos\theta}{2+X} \tag{20}$$

$$E_{vt} = -\left(\frac{1}{r} \frac{\partial V_v}{\partial \theta} \right)_{r=R} = -\frac{3E_0 \sin\theta}{2+X} \tag{21}$$

If the liquid–vapour interface supports no electrical free charges, it is shown [20] that the same equations, as written above, are obtained by replacing X with

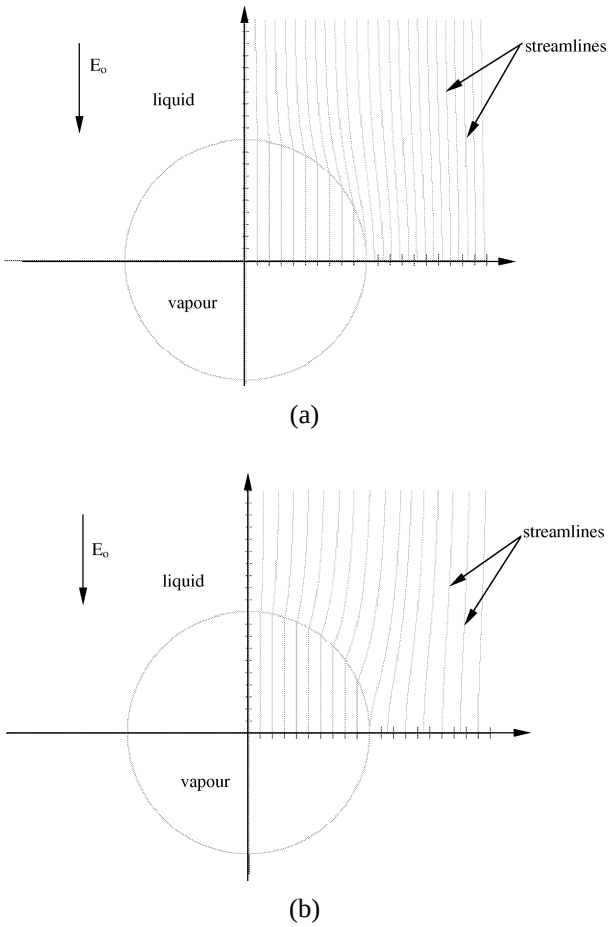

Figure 3. Electric field streamlines within and around a spherical bubble. (a) Dielectric bubble, (b) conducting bubble.

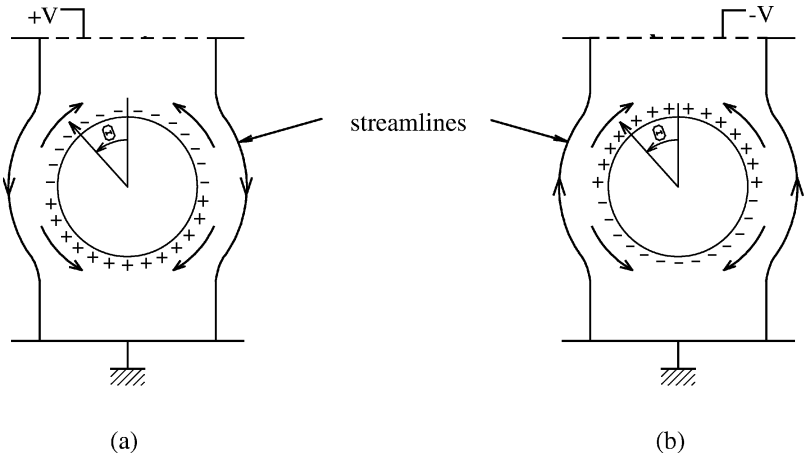

Figure 4. Electric field direction effect on the electrical free charge distribution at the bubble interface.

$1/Y = \varepsilon_v/\varepsilon_l$. In *figure 3a* are given the electric field distributions within and around a spherical dielectric bubble ($1/Y = 0.5,\ R = 1$ mm) for a 5 kV·cm^{-1} electric field strength. In the vapour phase, the electric field is uniform. However, in the liquid phase, near the liquid–vapour interface, there is an electric field distortion due to the presence of the bubble. Far away from the bubble, the electric field is uniform and its strength is equal to that of the applied electric field. In *figure 3b* are given the electric field distributions within and around a spherical conducting bubble ($X = 0.25,\ R = 1$ mm) for the same applied electric field strength E_0 as in the previous case. The electric field streamlines have a tendency to be normal to the liquid–vapour interface.

The appearance of free electrical charges at the liquid–vapour interface is due to a discontinuity of the normal electric field component. The electrical charge density is

$$q_s = \varepsilon_0\varepsilon_{rl}\left(\frac{\partial V_v}{\partial r}\right)_{r=R} - \varepsilon_0\varepsilon_{rv}\left(\frac{\partial V_l}{\partial r}\right)_{r=R} = 3\varepsilon_0\varepsilon_{rv}E_0\cos\theta\left(\frac{YX-1}{2+X}\right) \quad (22)$$

where $Y = \varepsilon_{rl}/\varepsilon_{rv} = \varepsilon_l/\varepsilon_v$.

The sign of the electrical free charges depends on the electric field direction, the electric field strength and the product of the liquid to vapour permittivity ratio, Y and that of electrical resistivity, X. When the electric field is directed towards the heat transfer surface (positive polarity) and if $XY < 1$, the bubble tip surface bears electrical free charges opposite in sign to the electrode that it faces (*figure 4a*). On the other hand, if $XY > 1$, the bubble tip surface bears electrical free charges of the same sign as the electrode that it faces. At the opposite, if the electric field direction is inverted (negative polarity), the electrical free charges distribution on the bubble interface is also inverted (*figure 4b*).

3.2. Electric stress expressions

The normal and the tangential components of the electric stress acting on a conducting bubble are expressed as follows (see Appendix):

$$f_{sn} = \frac{9\varepsilon_0E_0^2}{2(2+X)^2}\left[\frac{(\varepsilon_{rl}-1)^2}{3} + \left\{\left(\frac{\varepsilon_{rl}^2+4\varepsilon_{rl}-2}{3}\right)X^2 - \left(\frac{\varepsilon_{rl}^2-2\varepsilon_{rl}+4}{3}\right)\right\}\cos^2\theta\right] \quad (23)$$

$$f_{st} = -\frac{9\varepsilon_0\varepsilon_{rv}E_0^2}{(2+X)^2}(YX-1)\sin\theta\cos\theta \quad (24)$$

The normal electric stress can be rewritten in the following form (see Appendix):

$$f_{sn} = \frac{9\varepsilon_0E_0^2}{2(2+X)^2}(\alpha\cos^2\theta - \beta) \quad (25)$$

where

$$\alpha = \left(\frac{\varepsilon_{rl}^2+4\varepsilon_{rl}-2}{3}\right)X^2 - \left(\frac{\varepsilon_{rl}^2-2\varepsilon_{rl}+4}{3}\right)$$
$$\beta = -\frac{(\varepsilon_{rl}-1)^2}{3} \quad (26)$$

The normal components of f_{sn} acting on the bubble interface can be decomposed into horizontal and vertical

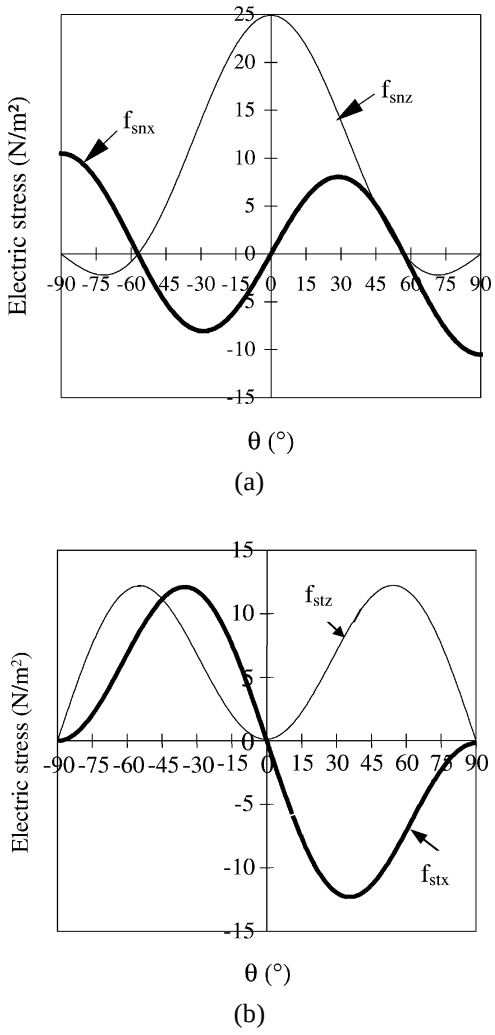

Figure 5. Electric stresses acting on a conducting bubble interface. (a) Normal electric stresses, (b) tangential electric stresses.

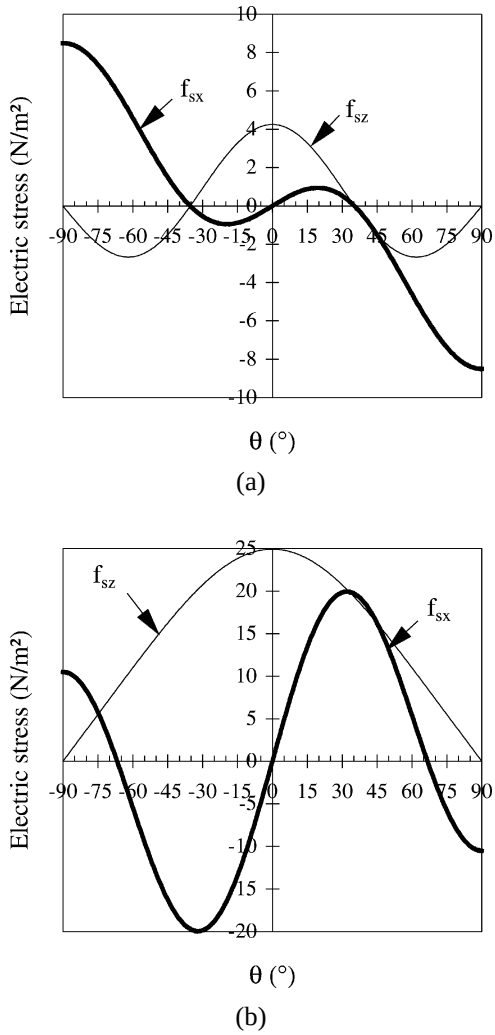

Figure 6. Horizontal and vertical components of the electric stresses. (a) Dielectric bubble, (b) conducting bubble.

ones, f_{snx} and f_{snz}, respectively. Variations of f_{snx} and f_{snz} along the liquid–vapour interface, for $E_0 = 20$ kV·cm^{-1}, are plotted as a function of the angular coordinate θ in *figure 5a*. The electrical resistivities ratio X is equal to 0.25. The horizontal component strength is maximum at the bubble equator where it is directed towards the vapour phase and contributes to the compression of the bubble. The vertical component strength is maximum at the bubble tip where it is directed towards the liquid phase and contributes to the bubble elongation in the electric field direction. The f_{stx} and f_{stz} variations are plotted against the angular coordinate θ in *figure 5b*. No tangential electric stresses act on the bubble equator ($\theta = \pm 90°$) or on the bubble tip ($\theta = 0°$) because there is no electrical free charge density on these locations. The horizontal component f_{stx}, directed towards the vapour phase, has a maximum value for $\theta \approx 35°$ and a minimum one for $\theta \approx -35°$. The vertical component f_{stz}, directed towards the liquid phase, presents two maxima at $\theta = \pm 55°$. The tangential electric stress direction, f_{st}, can be deduced from f_{stx} and f_{stz} variations. This is obvious since the bubble tip bears negative electrical free charges (the bubble tip faces the positive electrode) and the electric field direction is the same as the gravitational force, the Coulomb stress (f_{st} stress) generated on the bubble interface is opposite to the electric field direction as it is shown in *figure 4a*. *Figure 6a* represents f_{sx} and f_{sz} as a function of θ for a dielectric bubble (no electrical free

charge density at the bubble interface, $Y = 2$) submitted to a 20 kV·cm^{-1} electric field strength. The bubble is compressed strongly near the equator ($\theta = \pm 90°$) because the horizontal component of the electric stress is stronger than the vertical one. In *figure 6b* are shown the horizontal and vertical components of the electric stresses acting on a conducting bubble ($X = 0.25$).

For a dielectric bubble as well as a conducting bubble, the normal electric stress causes a distortion of the bubble. Whereas, the tangential electric stress, which is the Coulomb stress, acts if the bubble interface bears electrical free charges and it induces liquid movements around the bubble and vapour movements within the bubble. In the next section both the distortion and the induced electroconvective movements are studied for a conducting bubble immersed in an isothermal dielectric liquid.

4. ELECTROCONVECTIVE MOVEMENTS AROUND AND WITHIN A CONDUCTING BUBBLE

The immersed-bubble problem is solved on the basis of the creeping flow approximation. The basic assumption of creeping flow, developed by Stokes [21], is that inertia terms can be neglected in the momentum equation. In such a flow, with stream velocity U and body length L, pressure cannot scale with the dynamic term (ρU^2) but rather must depend upon a viscous term ($\mu U/L$). If the Reynolds number is small ($Re \ll 1$, e.g., inertia terms are negligible), the momentum equation which represents the creeping flow is

$$\nabla P = \mu \nabla^2 \boldsymbol{u} \tag{27}$$

to be combined with the incompressible continuity relation (equation (7)).

By taking the curl of the above equation, we obtain the useful relation

$$\nabla^2 \omega = 0 \tag{28}$$

where $\omega = \operatorname{curl} \boldsymbol{u}$ is the vorticity vector. Thus the vorticity satisfies Laplace's equation in a creeping flow. In two-dimensional Stokes flow, we can write [21]

$$\omega = -\nabla^2 \psi \tag{29}$$

where ψ is the stream function. The vorticity equation (equation (28)) may be rewritten as

$$\nabla^4 \psi = 0 \tag{30}$$

ψ is called biharmonic equation. In spherical coordinates, equation (30) is written

$$\left[\frac{\partial^2}{\partial r^2} + \frac{\sin\theta}{r^2}\frac{\partial}{\partial\theta}\left(\frac{1}{\sin\theta}\frac{\partial}{\partial\theta}\right)\right]^2 \psi = 0 \tag{31}$$

This equation allows the determination of the velocity profiles in both phases.

4.1. Velocity profiles in liquid and vapour phases

The normal and tangential velocity components u and v are related to the Stokes stream function ψ by

$$u = \frac{1}{r^2 \sin\theta}\frac{\partial\psi}{\partial\theta} \qquad v = -\frac{1}{r\sin\theta}\frac{\partial\psi}{\partial r} \tag{32}$$

In order to solve equation (31), solutions can be found by assuming the following form:

$$\psi = r^n \sin^2\theta \cos\theta \tag{33}$$

The solutions of equation (31) for the flow outside and inside the bubble are respectively

$$\begin{aligned} \psi_\mathrm{l} &= \left(A\frac{R^4}{r^2} + BR^2\right)\sin^2\theta\cos\theta \\ \psi_\mathrm{v} &= \left(C\frac{r^3}{R} + D\frac{r^5}{R^3}\right)\sin^2\theta\cos\theta \end{aligned} \tag{34}$$

The constants A, B, C and D whose dimension is a velocity are determined by the following boundary conditions written at the liquid–vapour interface

$$\begin{aligned} u_\mathrm{l} &= u_\mathrm{v} = 0 \\ v_\mathrm{l} &= v_\mathrm{v} \end{aligned} \tag{35}$$

These equations allow for

$$A = -B = C = -D = U^* \tag{36}$$

U^* has the dimension of a velocity.

By considering equation (36), the radial and orthoradial velocities in the liquid phase are given by

$$\begin{aligned} u_\mathrm{l} &= \frac{U^* R^2}{r^2}\left(\frac{R^2}{r^2} - 1\right)\left(3\cos^2\theta - 1\right) \\ v_\mathrm{l} &= \frac{2U^* R^4}{r^4}\sin\theta\cos\theta \end{aligned} \tag{37}$$

In the vapour phase, the radial and orthoradial velocities are expressed as follows:

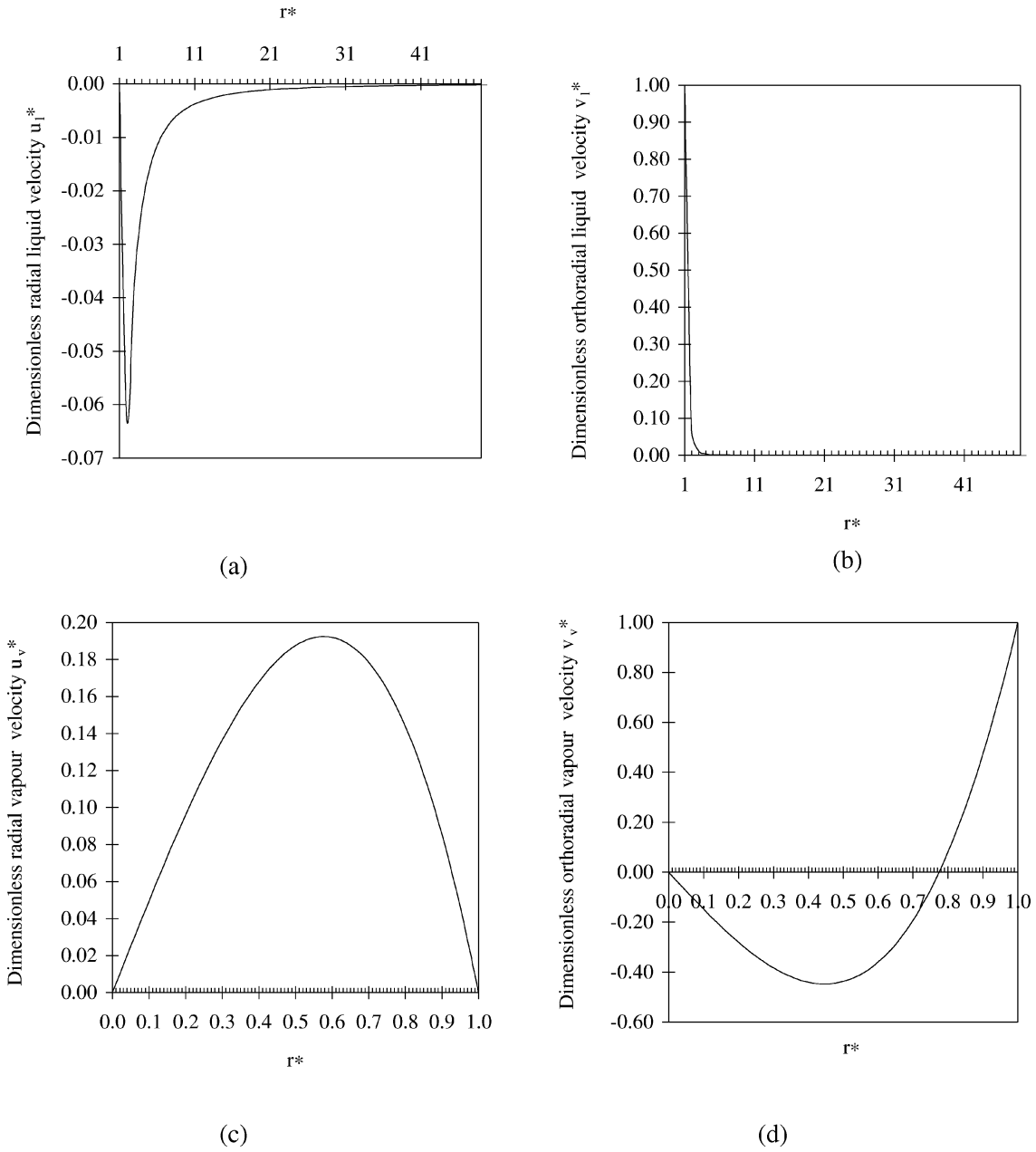

Figure 7. Velocity distributions within and around a conducting bubble. (a) Radial liquid velocity, (b) orthoradial liquid velocity, (c) radial vapour velocity, (d) orthoradial vapour velocity.

$$u_{\mathrm{v}} = \frac{U^* r}{R}\left(1 - \frac{r^2}{R^2}\right)\left(3\cos^2\theta - 1\right)$$
$$v_{\mathrm{v}} = -\frac{U^* r}{R}\left(3 - \frac{5r^2}{R^2}\right)\sin\theta\cos\theta \qquad (38)$$

The radial and orthoradial velocities are shown in *figure 7* as a function of the dimensionless radius r^* for $\theta = \pi/4$. In *figure 7a*, the radial velocity u_{l} in the liquid phase, directed towards the vapour phase, decreases from the zero value at the bubble interface (boundary condition) to a negative minimum value. Then, u_{l} increases and tends to

zero far away from the bubble interface. v_l variations are shown as a function of r^* in *figure 7b*. v_l decreases from its maximum value at the liquid–vapour interface to zero far away from the bubble. It appears that, near the bubble interface, the v_l values are higher than those of u_l. So, the electroconvective movements around the bubble interface are mainly due to the orthoradial component of the liquid velocity. The radial vapour velocity, u_v, is shown as a function of r^* in *figure 7c*. It increases from the bubble centre, reaches a maximum value and decreases to the zero value at the bubble interface (boundary condition). The orthoradial vapour velocity, v_v, decreases to a negative minimum value (*figure 7d*), then it increases to its maximum value U^* at the bubble interface.

These velocity profiles in the liquid and vapour phases are completely defined by the knowledge of the velocity U^*. This will be done by considering a force balance at the liquid–vapour interface.

4.2. Force balance at the liquid–vapour interface

The forces acting on the liquid–vapour interface are mainly the electric forces and the viscous forces (the inertia forces are negligible in the creeping flow approximation). The electric stresses are determined in Section 3.2. The normal and tangential viscous stresses acting on the liquid–vapour interface are

$$f_{visn} = -P + 2\mu\frac{\partial u}{\partial r} \tag{39}$$

$$f_{vist} = \mu\left(r\frac{\partial}{\partial r}\left(\frac{v}{r}\right) + \frac{1}{r}\frac{\partial u}{\partial \theta}\right) \tag{40}$$

P, the pressure acting on the liquid phase or the vapour phase, is determined by integrating the momentum equations

$$-\nabla P_l + \rho_l \boldsymbol{g} + \mu_l \nabla^2 \boldsymbol{u}_l = 0 \tag{41}$$

$$-\nabla P_v + \rho_v \boldsymbol{g} + \mu_v \nabla^2 \boldsymbol{u}_v = 0 \tag{42}$$

and the following expressions are obtained:

$$P_l = \Pi_l - \rho_l g r\cos\theta - \frac{2U^*R^2}{r^3}\mu_l\left(3\cos^2\theta - 1\right) \tag{43}$$

$$P_v = \Pi_v - \rho_v g r\cos\theta - \frac{7U^*r^2}{R^3}\mu_v\left(3\cos^2\theta - 1\right) \tag{44}$$

where Π_l and Π_v are the zero-field hydrostatic liquid and vapour pressures.

Thus, the normal viscous stresses are

$$f_{visnl} = -\Pi_l + \rho_l g r\cos\theta + \frac{2U^*R^2}{r^3}\mu_l\left[1 - \frac{4R^2}{r^2}\right]\left(3\cos^2\theta - 1\right) \tag{45}$$

$$f_{visnv} = -\Pi_v + \rho_v g r\cos\theta + \frac{U^*}{R}\mu_v\left[2 + \frac{r^2}{R^2}\right]\left(3\cos^2\theta - 1\right) \tag{46}$$

The tangential viscous stresses in each phase are given by equation (40)

$$f_{vistl} = \mu_l\left(-16\frac{R^4}{r^5} + 6\frac{R^2}{r^3}\right)U^*\sin\theta\cos\theta \tag{47}$$

$$f_{vistv} = \mu_v\left(16\frac{r^2}{R^3} - \frac{6}{R}\right)U^*\sin\theta\cos\theta \tag{48}$$

The equilibrium equations to be satisfied at the liquid–vapour interface are

$$f_{st}\big|_{r=R} + f_{vistl}\big|_{r=R} - f_{vistv}\big|_{r=R} = 0 \tag{49}$$

$$f_{sn}\big|_{r=R} + f_{visnl}\big|_{r=R} - f_{visnv}\big|_{r=R} + \sigma\left(\frac{1}{r_1} + \frac{1}{r_2}\right) = 0 \tag{50}$$

σ is the surface tension while r_1 and r_2 are the principal radii of curvature.

The balance of tangential stresses is written by considering equations (47)–(49)

$$-\frac{9\varepsilon_0\varepsilon_{rv}E_0^2}{(2+X)^2}(YX-1)\sin\theta\cos\theta - 10\frac{U^*}{R}(\mu_l+\mu_v)\sin\theta\cos\theta = 0 \tag{51}$$

From this equation, an expression of the velocity U^* is obtained as a function of the applied electric field E_0, the dielectric permittivities, the electrical conductivities and the dynamic viscosities of each phase

$$U^* = -\frac{9\varepsilon_0\varepsilon_{rv}E_0^2(XY-1)R}{10(\mu_l+\mu_v)(2+X)^2} \tag{52}$$

U^* is the maximum liquid velocity which occurs at $\theta = \pi/4$ on the bubble interface.

The maximum liquid velocity depends on the square of the electric field strength and therefore does not depend on the electric field polarity. Indeed, when the polarity is inverted, the electric field direction and the electrical free charges on the liquid–vapour interface are also inverted. As a result, the Coulomb forces have the same orientation and the liquid movement around the bubble is unchanged (*figure 2*). The liquid flows from

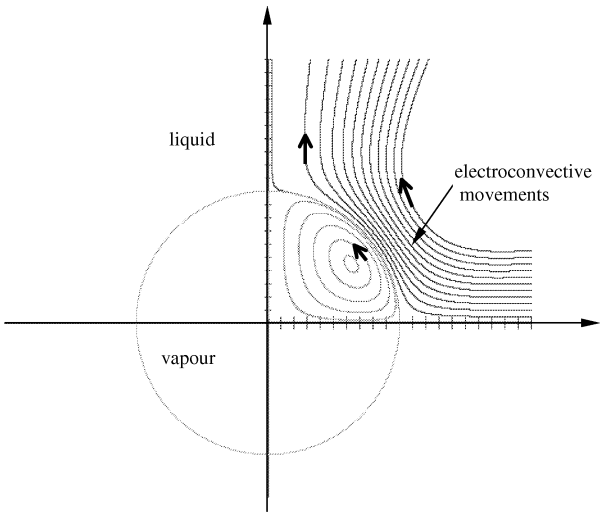

Figure 8. Electroconvective movements within and around a conducting bubble.

the bubble tip to the equator. The streamlines are shown in *figure 8*, for a 5 kV·cm^{-1} electric field strength. The electroconvective movement direction, which is indicated by arrows, is the same as that of the tangential electric stresses (Coulomb stresses) and depends only on the product XY. For the bubble, this product is generally lower than 1.

From equations (45), (46) and (50), the equilibrium of the normal stresses is as follows:

$$\sigma\left[\frac{1}{r_1}+\frac{1}{r_2}\right]=(\Pi_v-\Pi_l)-(\rho_l-\rho_v)gR\cos\theta + \frac{3(2\mu_l+\mu_v)}{R}U^*\left(3\cos^2\theta-1\right) - \frac{9\varepsilon_0E_0^2(\alpha\cos^2\theta-\beta)}{2(2+X)^2} \tag{53}$$

By considering the hydrostatic pressure difference $(\Pi_v-\Pi_l)$ equal to $2\sigma/R$, we obtain

$$\sigma\left[\frac{1}{r_1}+\frac{1}{r_2}\right]=\frac{2\sigma}{R}-(\rho_l-\rho_v)gR\cos\theta + \frac{3(2\mu_l+\mu_v)}{R}U^*\left(3\cos^2\theta-1\right) - \frac{9\varepsilon_0E_0^2(\alpha\cos^2\theta-\beta)}{2(2+X)^2} \tag{54}$$

This relation can be rewritten by considering the Legendre polynomials, P_n:

$$\sigma\left[\frac{1}{r_1}+\frac{1}{r_2}\right]=a_0P_0(\cos\theta)+a_1P_1(\cos\theta)+a_2P_2(\cos\theta) \tag{55}$$

where

$$a_0=\frac{2\sigma}{R}+\frac{3(3\beta-\alpha)\varepsilon_0E_0^2}{2(2+X)^2}$$
$$a_1=-(\rho_l-\rho_v)gR \tag{56}$$
$$a_2=-\frac{3\varepsilon_0E_0^2}{(2+X)^2}\left[\frac{9}{5}\frac{2\mu_l+\mu_v}{\mu_l+\mu_v}(\varepsilon_lX-\varepsilon_v)+\alpha\right]$$

From equation (55), we can determine the bubble deformation in presence of an electric field. For small deviations from a spherical shape, we can express the deformation as

$$r=R+\zeta(\theta) \tag{57}$$

r is the local radius of curvature expressed as a function of the initial spherical bubble radius R and ζ is the bubble deformation that depends only on the angle θ. Thus we have

$$\frac{1}{r_1}+\frac{1}{r_2}=\frac{2}{R}-\frac{2\zeta}{R^2}-\frac{1}{R^2}\left(\frac{1}{\sin\theta}\frac{\partial}{\partial\theta}\left(\sin\theta\frac{\partial\zeta}{\partial\theta}\right)\right) \tag{58}$$

Putting $\zeta^*=\zeta/R,\ \mu^*=\cos\theta$, equation (58) is rewritten as

$$2-2\zeta^*-\frac{\mathrm{d}}{\mathrm{d}\mu^*}\left[\left(1-\mu^{*2}\right)\frac{\mathrm{d}\zeta^*}{\mathrm{d}\mu^*}\right]=\frac{R}{\sigma}\sum_{n=0}^{2}a_nP_n(\mu^*) \tag{59}$$

This equation may be solved to express the deformation simply in terms of the coefficients

$$\zeta^*=\frac{R}{\sigma}\sum_{n=2}\frac{a_nP_n(\mu^*)}{(2+n)(1-n)} \tag{60}$$

The comparison between the bubble shapes with and without electroconvective movements is shown in *figure 9* for 5 kV·cm^{-1} and 10 kV·cm^{-1} electric field strengths. For these numerical results, the dielectric permittivities ratio is equal to 1.8 (case of *n*-pentane) and the electrical conductivities ratio to 1. Initial spherical bubble radius is 1 mm. For a 10 kV·cm^{-1} electric field strength, the bubble shape is not ellipsoidal as for the liquid–vapour interface without electrical free charges. Also, it is predicted that the bubble deformation is more pronounced in the presence of electroconvective movements. The bubble deformation is shown in *figure 10* for different values of the product XY. In these calculations, $X=1.8$ and Y varies from 1 to 4. The results show the greatest bubble elongation for the highest value of Y.

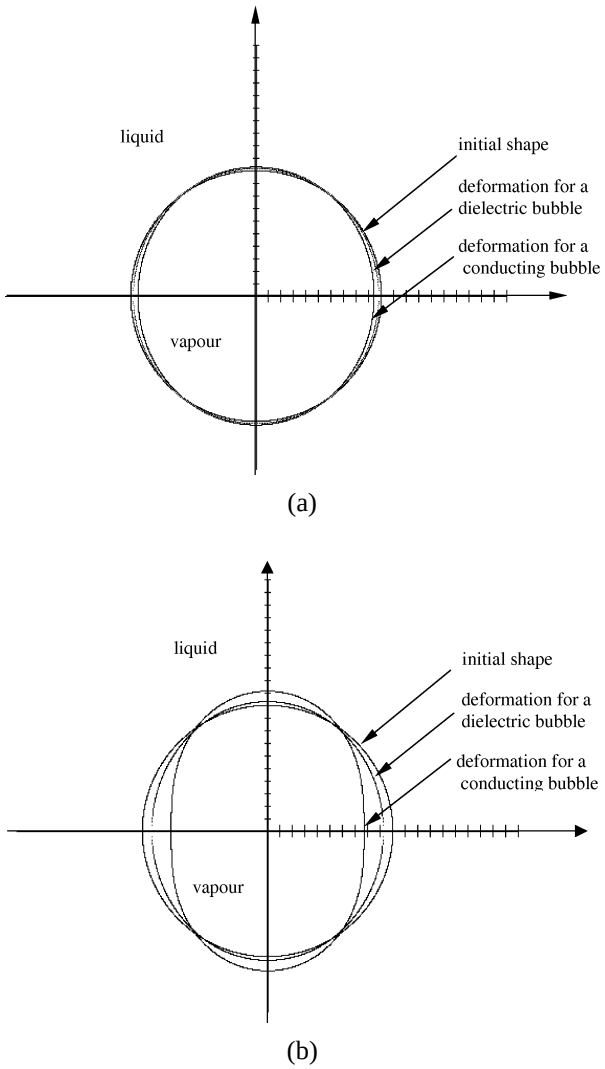

Figure 9. Deformation of a dielectric and a conducting bubble under a DC electric field. (a) $E_0 = 5$ kV·cm^{-1}, (b) $E_0 = 10$ kV·cm^{-1}.

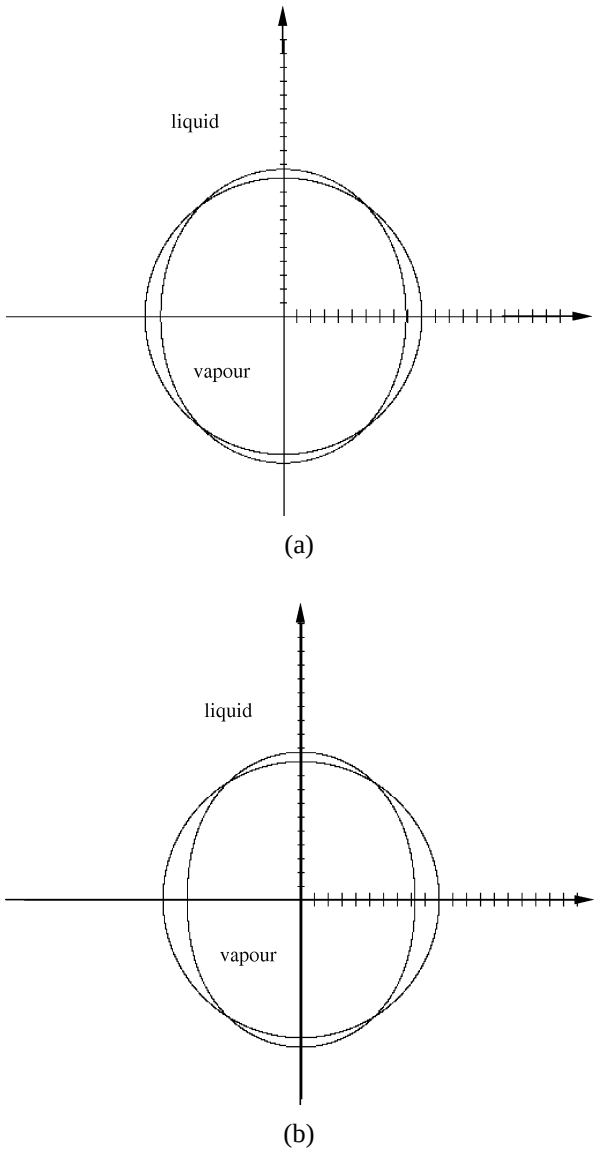

Figure 10. Effect of the electrical conductivity on the bubble deformation.

5. CONCLUSION

We have investigated the effects of a uniform electric field on bubbles. The electric stresses acting on conducting bubbles are analysed and compared with those acting on dielectric bubbles. The normal electric stresses cause a distortion of the bubble in the electric field direction. Whereas, the tangential electric stresses, which are the Coulomb forces, induce liquid movements around the bubble and vapour movements within the bubble. The electroconvective movements are analysed on the basis of the creeping flow approximation. Thus, the momentum equations are solved analytically. The balance of tangential stresses in the presence of electroconvective movements leads to a determination of a maximum liquid velocity around the bubble. The equilibrium of the normal stresses allows for a determination of the bubble deformation. Numerical simulations are done in order to compare the bubble shape with and without electroconvective movements. It is shown that the bubble deformation is more pronounced in the presence of electroconvective movements. The bubble elongation depends on the dielectric permittivities as well as the electrical conductivities.

REFERENCES

[1] Jones T.B., Electrohydrodynamically enhanced heat transfer in liquids—A review, Advances in Heat Transfer 14 (1978) 107–148.

[2] Allen P.H.G., Karayiannis T.G., Electrohydrodynamic enhancement of heat transfer and fluid flow, Heat Recovery Systems & CHP 15 (5) (1995) 389–423.

[3] Ohadi M.M., Sharaf N., Nelson D.A., Electrohydrodynamic enhancement of heat transfer in a shell-and-tube heat exchanger, Experimental Heat Transfer 14 (1991) 19–39.

[4] Damianidis C., Karayiannis T.G., Al-Dadah R.K., James R.W., Collins M.W., Allen P.H.G., EHD boiling enhancement in shell-and-tube evaporators and its application in refrigeration plants, ASHRAE Trans. Symp. 98, Part II, 1992, pp. 462–472.

[5] Zaghdoudi M.C., Cioulachtjian S., Lallemand M., EHD enhancement of pool boiling of pentane on a horizontal copper surface, in: Int. Symp. on Two-phase Flow Modelling and Experimentation, October, Roma, Italy, 1995, pp. 1075–1082.

[6] Zaghdoudi M.C., Lallemand M., Study of the EHD effect on heat transfer with boiling dielectric fluids, in: International Symposium on the physics of Heat and Mass Transfer in Boiling and Condensation, Moscow, Russia, 21–24 May 1997, pp. 335–340.

[7] Zaghdoudi M.C., Lallemand M., Effet d'un champ électrique sur le phénomène d'hystérésis en ébullition nucléée, in: Congrès de la Société Française des Thermiciens, Poitiers, France, 17–19 Mai 1995, pp. 337–342.

[8] Berghmans J., Electrostatic fields and the maximum heat flux, Int. J. Heat Mass Transfer 19 (1976) 791–797.

[9] Garton C.G., Krasucki Z., Bubbles in insulating liquids: stability in an electric field, Proc. Roy. Soc. London Ser. A 280 (1964) 211–226.

[10] Miksis M.J., Shape of a drop in an electric field, Phys. Fluids 24 (11) (1981) 1967–1972.

[11] Cheng K.J., Chaddock J.B., Maximum size of bubbles during nucleate boiling in an electric field, Int. J. Heat Fluid Flow 7 (4) (1986) 278–282.

[12] Ogata J., Yabe A., Basic study on the enhancement of nucleate boiling heat transfer by applying electric fields, Int. J. Heat Mass Transfer 36 (3) (1993) 278–282.

[13] Cho H.J., Kang I.S., Kweon Y.C., Kim M.H., Study of the behavior of a bubble attached to a wall in a uniform electric field, Int. J. Multiphase Flow 22 (5) (1996) 909–922.

[14] Kweon Y.C., Kim M.H., Cho H.J., Kang Y.S., Study on the deformation and departure of a bubble attached to a wall in DC/AC electric fields, Int. J. Multiphase Flow 24 (1) (1998) 145–162.

[15] Ogata J., Yabe A., Augmentation of nucleate boiling heat transfer by applying electric fields: EHD behavior of boiling bubble, in: Proceedings of ASME-JSME Thermal Engineering 3, 1991, pp. 41–46.

[16] Ogata J., Yabe A., Augmentation of boiling heat transfer by utilizing the EHD effect—EHD behaviour of boiling bubbles and heat transfer characteristics, Int. J. Heat Mass Transfer 36 (3) (1993) 783–791.

[17] Jones T.B., Hallock K.R., Surface wave model of electrohydrodynamically coupled minimum film boiling, Journal of Electrostatics 5 (1978) 273–284.

[18] Jones T.B., Schaeffer R.C., Electrohydrodynamically coupled minimum film boiling in dielectric liquids, AIAAJ 14 (1976) 1759–1765.

[19] Durand E., Méthodes de calcul des diélectriques, Electrostatique III, Masson et C^{ie}, Paris, 1966.

[20] Zaghdoudi M.C., Amélioration des transferts de chaleur en ébullition sous l'action d'un champ électrique, Thèse de Doctorat, INSA, Lyon, France, 1996.

[21] White F.M., Viscous fluid flow, in: Beamesderfer L. and Morriss J.M. (Eds.), McGraw-Hill International Editions, Singapore, 1991.

APPENDIX

Electric stresses acting on the liquid–vapour interface

1. Electric stresses acting on a nonconducting bubble

The interfacial electric force acting on each phase j is expressed as follows:

$$\boldsymbol{f}_{\mathrm{s}j} = \varepsilon_j (\boldsymbol{n}\cdot\boldsymbol{E})_j \boldsymbol{E}_j - \frac{\varepsilon_j}{2} E_j^2 \left(1 - \frac{\rho}{\varepsilon}\frac{\partial\varepsilon}{\partial\rho}\right)_j \boldsymbol{n}_j \quad \text{(A.1)}$$

The force resultant $\boldsymbol{f}_{\mathrm{s}}$ acting on the liquid–vapour interface is

$$\begin{aligned}
\boldsymbol{f}_{\mathrm{s}} &= \left\{\varepsilon_{\mathrm{l}}(\boldsymbol{n}\cdot\boldsymbol{E})_{\mathrm{l}}\boldsymbol{E}_{\mathrm{l}} - \frac{\varepsilon_{\mathrm{l}}}{2}E_{\mathrm{l}}^2\left(1 - \frac{\rho_{\mathrm{l}}}{\varepsilon_{\mathrm{l}}}\frac{\mathrm{d}\varepsilon_{\mathrm{l}}}{\mathrm{d}\rho_{\mathrm{l}}}\right)\boldsymbol{n}_{\mathrm{l}}\right\} \\
&\quad + \left\{\varepsilon_{\mathrm{v}}(\boldsymbol{n}\cdot\boldsymbol{E})_{\mathrm{v}}\boldsymbol{E}_{\mathrm{v}} - \frac{\varepsilon_{\mathrm{v}}}{2}E_{\mathrm{v}}^2\left(1 - \frac{\rho_{\mathrm{v}}}{\varepsilon_{\mathrm{v}}}\frac{\mathrm{d}\varepsilon_{\mathrm{v}}}{\mathrm{d}\rho_{\mathrm{v}}}\right)\boldsymbol{n}_{\mathrm{v}}\right\} \\
\boldsymbol{f}_{\mathrm{s}} &= \left\{\varepsilon_{\mathrm{l}}E_{\mathrm{ln}}(E_{\mathrm{ln}}\boldsymbol{n}_{\mathrm{l}} + E_{\mathrm{lt}}\boldsymbol{t}_{\mathrm{l}}) - \frac{\varepsilon_{\mathrm{l}}}{2}E_{\mathrm{l}}^2\left(1 - \frac{\rho_{\mathrm{l}}}{\varepsilon_{\mathrm{l}}}\frac{\mathrm{d}\varepsilon_{\mathrm{l}}}{\mathrm{d}\rho_{\mathrm{l}}}\right)\boldsymbol{n}_{\mathrm{l}}\right\} \\
&\quad + \left\{\varepsilon_{\mathrm{v}}E_{\mathrm{vn}}(E_{\mathrm{vn}}\boldsymbol{n}_{\mathrm{v}} + E_{\mathrm{vt}}\boldsymbol{t}_{\mathrm{v}})\right. \\
&\quad \left. - \frac{\varepsilon_{\mathrm{v}}}{2}E_{\mathrm{v}}^2\left(1 - \frac{\rho_{\mathrm{v}}}{\varepsilon_{\mathrm{v}}}\frac{\mathrm{d}\varepsilon_{\mathrm{v}}}{\mathrm{d}\rho_{\mathrm{v}}}\boldsymbol{n}_{\mathrm{v}}\right)\right\} \\
\boldsymbol{f}_{\mathrm{s}} &= \left\{\varepsilon_{\mathrm{l}}E_{\mathrm{ln}}^2\boldsymbol{n}_{\mathrm{l}} + \varepsilon_{\mathrm{l}}E_{\mathrm{ln}}E_{\mathrm{lt}}\boldsymbol{t}_{\mathrm{l}}\right. \\
&\quad \left. - \frac{\varepsilon_{\mathrm{l}}}{2}(E_{\mathrm{ln}}^2 + E_{\mathrm{lt}}^2)\boldsymbol{n}_{\mathrm{l}} + \frac{\rho_{\mathrm{l}}}{2}E_{\mathrm{l}}^2\frac{\mathrm{d}\varepsilon_{\mathrm{l}}}{\mathrm{d}\rho_{\mathrm{l}}}\boldsymbol{n}_{\mathrm{l}}\right\} \\
&\quad + \left\{\varepsilon_{\mathrm{v}}E_{\mathrm{vn}}^2\boldsymbol{n}_{\mathrm{v}} + \varepsilon_{\mathrm{v}}E_{\mathrm{vn}}E_{\mathrm{vt}}\boldsymbol{t}_{\mathrm{v}}\right. \\
&\quad \left. - \frac{\varepsilon_{\mathrm{v}}}{2}(E_{\mathrm{vn}}^2 + E_{\mathrm{vt}}^2)\boldsymbol{n}_{\mathrm{v}} + \frac{\rho_{\mathrm{v}}}{2}E_{\mathrm{v}}^2\frac{\mathrm{d}\varepsilon_{\mathrm{v}}}{\mathrm{d}\rho_{\mathrm{v}}}\boldsymbol{n}_{\mathrm{v}}\right\}
\end{aligned}$$

$$\boldsymbol{f}_s = \left\{ \frac{\varepsilon_l}{2}\left(E_{ln}^2 - E_{lt}^2\right)\boldsymbol{n}_l + \frac{\rho_l}{2}\frac{d\varepsilon_l}{d\rho_l}E_l^2\boldsymbol{n}_l + \frac{\varepsilon_v}{2}\left(E_{vn}^2 - E_{vt}^2\right)\boldsymbol{n}_v + \frac{\rho_v}{2}\frac{d\varepsilon_v}{d\rho_v}E_v^2\boldsymbol{n}_v \right\} + \{\varepsilon_l E_{ln}E_{lt}\boldsymbol{t}_l + \varepsilon_v E_{vn}E_{vt}\boldsymbol{t}_v\} \quad (A.2)$$

If we consider the relations

$$\begin{aligned} \boldsymbol{n}_l &= -\boldsymbol{n}_v \\ \boldsymbol{t}_l &= -\boldsymbol{t}_v \end{aligned} \quad (A.3)$$

equation (A.2) can be rewritten as

$$\boldsymbol{f}_s = \frac{1}{2}\left\{ \varepsilon_l\left(E_{ln}^2 - E_{lt}^2\right) - \varepsilon_v\left(E_{vn}^2 - E_{vt}^2\right) + \rho_l\frac{d\varepsilon_l}{d\rho_l}E_l^2 - \rho_v\frac{d\varepsilon_v}{d\rho_v}E_v^2 \right\}\boldsymbol{n}_l + \{\varepsilon_l E_{ln}E_{lt} - \varepsilon_v E_{vn}E_{vt}\}\boldsymbol{t}_l \quad (A.4)$$

For a nonconducting bubble without electrical charges at the liquid–vapour interface we have the following relations (continuity of the electric displacement):

$$\begin{aligned} \varepsilon_l \boldsymbol{E}_{ln} &= \varepsilon_v \boldsymbol{E}_{vn} \\ \boldsymbol{E}_{lt} &= \boldsymbol{E}_{vt} \end{aligned} \quad (A.5)$$

Therefore, equation (A.4) is written as

$$\boldsymbol{f}_s = \frac{1}{2}\left\{ \varepsilon_l\left(1 - \frac{\varepsilon_l}{\varepsilon_v}\right)E_{ln}^2 + (\varepsilon_v - \varepsilon_l)E_{lt}^2 + \rho_l\frac{d\varepsilon_l}{d\rho_l}E_l^2 - \rho_v\frac{d\varepsilon_v}{d\rho_v}E_v^2 \right\}\boldsymbol{n}_l \quad (A.6)$$

Thus, $\boldsymbol{f}_s$ is a normal stress. For a nonpolar dielectric fluid, the above relation is expressed by considering the Clausius–Mossotti equation as

$$\boldsymbol{f}_{sn} = \frac{\varepsilon_0}{2}\left\{ \varepsilon_{rl}(1-\varepsilon_{rl})E_{ln}^2 + (1-\varepsilon_{rl})E_{lt}^2 + \frac{(\varepsilon_{rl}-1)(\varepsilon_{rl}+2)}{3}E_l^2 \right\}\boldsymbol{n}_l \quad (A.7)$$

or

$$\boldsymbol{f}_{sn} = \varepsilon_0\left\{ -\frac{(\varepsilon_{rl}-1)^2}{3}E_{ln}^2 + \frac{(\varepsilon_{rl}-1)^2}{6}E_{lt}^2 \right\}\boldsymbol{n}_l = -\varepsilon_0\frac{(\varepsilon_{rl}-1)^2}{6}\left\{2E_{ln}^2 - E_{lt}^2\right\}\boldsymbol{n}_l \quad (A.8)$$

2. Electric stresses acting on a conducting bubble

The normal electric stress is

$$f_{sn} = \frac{\varepsilon_0}{2}\left\{ \varepsilon_{rl}\left(E_{ln}^2 - E_{lt}^2\right) - \varepsilon_{rv}\left(E_{vn}^2 - E_{vt}^2\right) + \frac{(\varepsilon_{rl}-1)(\varepsilon_{rl}+2)}{3}E_l^2 \right\} \quad (A.9)$$

By considering equations (18), (19), (20) and (21), the following equations can be written:

$$\begin{cases} E_l^2 = \dfrac{9E_0^2}{(2+X)^2}\left[X^2\cos^2\theta + \sin^2\theta\right] \\ E_v^2 = \dfrac{9E_0^2}{(2+X)^2} \end{cases} \quad (A.10)$$

$$\begin{cases} E_{ln}^2 - E_{lt}^2 = \dfrac{9E_0^2}{(2+X)^2}\left[X^2\cos^2\theta - \sin^2\theta\right] \\ E_{vn}^2 - E_{vt}^2 = \dfrac{9E_0^2}{(2+X)^2}\left[\cos^2\theta - \sin^2\theta\right] \end{cases} \quad (A.11)$$

Then, the normal component of the electric stress acting on the liquid–vapour interface is

$$f_{sn} = \frac{9\varepsilon_0 E_0^2}{2(2+X)^2}\left[\varepsilon_{rl}\left(X^2\cos^2\theta - \sin^2\theta\right) - \left(\cos^2\theta - \sin^2\theta\right) + \frac{(\varepsilon_{rl}-1)(\varepsilon_{rl}+2)}{3}\left[X^2\cos^2\theta + \sin^2\theta\right] \right]$$

or

$$f_{sn} = \frac{9\varepsilon_0 E_0^2}{2(2+X)^2}\left[\frac{(\varepsilon_{rl}-1)^2}{3} + \left\{ \left(\frac{\varepsilon_{rl}^2 + 4\varepsilon_{rl} - 2}{3}\right)X^2 - \left(\frac{\varepsilon_{rl}^2 - 2\varepsilon_{rl} + 4}{3}\right) \right\}\cos^2\theta \right]$$